Journal of Controlled Release 319 (2020) 234–245

Contents lists available at ScienceDirect

Journal of Controlled Release

journal homepage: www.elsevier.com/locate/jconrel

Controlled release of adenosine from core-shell nanofibers to promote bone regeneration through STAT3 signaling pathway

Xin Cheng[a,1], Gu Cheng[a,b,1], Xin Xing[a], Chengcheng Yin[a], Yuet Cheng[a], Xue Zhou[c], Shan Jiang[d], Fenghua Tao[e], Hongbing Deng[b,*], Zubing Li[a,*]

[a] The State Key Laboratory Breeding Base of Basic Science of Stomatology (Hubei-MOST), Key Laboratory of Oral Biomedicine Ministry of Education, School & Hospital of Stomatology, Wuhan University, Wuhan 430079, China
[b] Hubei International Scientific and Technological Cooperation Base of Sustainable Resource and Energy, Hubei Key Lab of Biomass Resource Chemistry and Environmental Biotechnology, School of Resource and Environmental Science, Wuhan University, Wuhan 430079, China
[c] School of Public Health, Tongji Medical College, Huazhong University of Science and Technology, Wuhan 430030, China
[d] Department of Chemical and Biological Engineering, Iowa State University, Ames, IA 50014, USA
[e] Department of Orthopedics, Renmin Hospital of Wuhan University, Wuhan University, Wuhan 430060, China

ARTICLE INFO

Keywords:
Adenosine
Coaxial electrospinning
Nanofiber
Bone formation
STAT3 signaling pathway

ABSTRACT

Adenosine (Ade) has been identified to stimulate bone formation. However, the use of Ade is severely limited by the accompanying side effects and its very short half-life *in vivo*. This study aimed to fabricate an efficient drug-delivery system to reduce the undesirable side effects and enable the clinical application of Ade for treating large bone defects. The fabricated poly(ε-caprolactone) (PCL)/Ade-polyvinyl alcohol (PVA)$_{(0.3/0.4)}$ nanofibrous mats with 0.3:0.4 (w/w) ratio of Ade and PVA showed a sustained and controlled release of Ade and facilitated the osteogenic differentiation of bone mesenchymal progenitor cells (BMSCs). A larger amount of newly formed bone was observed *in vivo* in the cranial defects of the PCL/Ade-PVA$_{(0.3/0.4)}$ group compared with those of the non-loaded PCL/PVA nanofibrous mats at 4 and 8 weeks after surgery. Moreover, it is the first time to confirm that Ade mediates the osteogenesis of rat BMSCs through the STAT3 signaling pathway and restrains the osteoclastogenesis of rat bone-marrow macrophages (BMMs). These results suggested that this coaxial drug-delivery system loaded with Ade provided a promising and clinically relevant platform to controlled-release Ade and address large bone defects.

1. Introduction

The turbulence caused by pathological conditions such as infection, tumor resection, and trauma results in disrupted bone homeostasis, which render bone vulnerable to defect and fracture. As a ubiquitous purine nucleoside, adenosine (Ade) was produced intracellularly and extracellularly from the metabolism of adenosine-5′-triphosphate [1–3] and involved in bone homeostasis and bone regulation [4]. However, the side effects under systemic administration, such as restraint of cardiac function, decrease in blood pressure, and accumulation of hepatotoxicity, may severely limit the therapeutic impact of adenosine [5–7]. Moreover, excessive adenosine accumulation may lead to skeletal system disorders. The conditional knockout of ecto-adenosine deaminase (ecto-ADA), a ubiquitous catabolic enzyme on the cell surface responsible for the deamination of adenosine into inosine [8], resulted in reduced trabecular bone density in mice [9]. Adenosine has a very short half-life in the interstitial fluid due to the deamination of ecto-ADA, together with the phosphorylation of adenosine to adenosine monophosphate by adenosine kinase (ADK) [6], which acts like a feedback loop to limit the adenosine concentration and hinder its clinical application, although adenosine can be considerably generated under pathological conditions such as hypoxia or inflammation [10]. Therefore, traditional administration of adenosine also cannot attain a good curative effect due to this unique metabolism pathway.

In order to conquer these problems and explore the possible signaling pathway involved in adenosine-mediated osteogenesis, the *co*-axial poly(ε-caprolactone) (PCL)/polyvinyl alcohol (PVA) nanofibers with a sustained and controlled release of adenosine for the aim to reduce the undesirable side effects were fabricated in this study. By separating the organic solvents from the hydrosoluble biological

* Corresponding author.
E-mail addresses: hbdeng@whu.edu.cn (H. Deng), lizubing@whu.edu.cn (Z. Li).
[1] These authors contributed equally to this work.

https://doi.org/10.1016/j.jconrel.2019.12.048
Received 29 September 2019; Received in revised form 16 December 2019; Accepted 28 December 2019
Available online 30 December 2019
0168-3659/

molecules, the bioactivities of the loaded drugs can be perfectly maintained by the co-axial nanofibers [11,12]. Moreover, the controlled-release of adenosine can also be achieved by incorporation of adenosine into the inner layer of the coaxial nanofibers by adjusting the ratio of outer and inner materials. In our previous study, the coaxial silk fibroin/PCL/PVA nanofibrous mats have been successfully fabricated to facilitate bone repair. In this controlled-release system, bone morphogenetic protein 2 (BMP2)/PVA blending solution was embedded into the inner layer of the coaxial nanofibers and BMP2 exhibited a sustained release profile [13]. Therefore, we believe the coaxial nanofibers with controlled-release function of adenosine can conquer the disadvantages of the traditional adenosine-administrated methods by the technology of coaxial electrospinning.

Coaxial electrospinning utilizes a coaxial-nozzle configuration combining different biodegradable synthetic or natural polymers to take full advantage of the individual intrinsic advantages to manufacture coaxial fibers with unique core–sheath structure, which exhibits a highly aligned, porous, tubular, and hollow morphology. Previous study proved that coaxial nanofibers can not only control release but also preserve the bioactivities of the loaded- reagents [14,15]. Polylactic acid/collagen coaxial fibers with incorporated gentamicin have been reported to exhibit a sustained release of gentamicin and high antibacterial activity [16]. The encapsulation of bone morphogenetic protein 2 (BMP2) into poly(L-lactide-*co*-ε-caprolactone)/collagen coaxial fibers resulted in a controlled release profile and stable bioactivity for bone tissue regeneration [17].

Among all the preferable polymers commonly used in coaxial electrospinning, hydrophobic PCL has demonstrated excellent biocompatibility, and biodegradability [18–21]. PVA is also a biodegradable polymer and has been extensively studied in tissue engineering because of its hydrophilicity, thermal stability, and advantageous mechanical property [22–25]. In this study, we fabricated coaxial PCL/PVA nanofibers with adenosine incorporated inside the nanofibers and evaluated the sustained and controlled release of adenosine.

The potential molecular mechanism of adenosine to assist osteogenesis of bone mesenchymal progenitor cells (BMSCs) and the involved signaling pathway were also explored in this study. Adenosine mediates physiologic and pharmacologic effects by interacting with the G protein coupled P1 purinergic receptors (A1, A2A, A2B, and A3) located on the cell surface [26]. Most studies have shown that adenosine and its receptors are involved in bone homeostasis and bone regulation [27,28]. However, the molecular mechanisms downstream are not clearly understood. Here, the downstream molecular mechanism conducted by adenosine during osteogenesis and effects of the composite nanofibers on the regeneration of rat cranial defects were also investigated in this study (Scheme 1). By doing these, the undesirable side effects would be decreased and suitable application of adenosine in the bone regeneration would be attained.

2. Materials and methods

2.1. Cell culture and osteogenic or osteoclastogenic differentiation

4-week-old Sprague-Dawley (SD) rats were used in this study, and the long-bone MSCs were isolated according to previous protocols [29]. Then the harvested bone mesenchymal progenitor cells (BMSCs) from femurs and tibias were cultivated in α-MEM (Hyclone, Thermo Fisher Scientific, USA) supplemented with 10% fetal bovine serum (FBS; Gibco, Life Technologies Corporation, USA) and 1% penicillin/streptomycin (Hyclone, Thermo Fisher Scientific, USA) at 37 °C with 5% CO_2. Confluent cells from passages 3–6 were cultured in osteogenic differentiation medium consisting of α-MEM supplemented with 10% FBS, 1% penicillin/streptomycin, 10 nM dexamethasone (Sigma-Aldrich, St.Louis, USA), 50 μg/ml L-ascorbic acid (Sigma-Aldrich, St.Louis, USA), and 10 mM β-glycerophosphate (Sigma-Aldrich, St.Louis, USA), which was replaced every 2 days. For osteoclastogenic differentiation, BMMs were obtained according to our previous study [30]. Cells were cultured in DMEM (Hyclone, Thermo Fisher Scientific, USA) supplemented with 10% FBS and 1% penicillin/streptomycin at 37 °C with 5% CO_2, and additionally with M-CSF (50 ng/ml; PeproTech, USA) and RANKL (50 ng/ml; PeproTech, USA). The medium was replaced every 2 days.

2.2. Cell viability determined using the CCK8 assay

Cell viability was evaluated using a CCK8 kit (Dojindo, Kyushu Island, Japan). Briefly, BMSCs (5000 cells/well) were seeded in 96-well plates (Corning, Albany, USA) and were co-cultured with different concentrations of adenosine (Sigma-Aldrich, St.Louis, USA; 15 μg/ml, 30 μg/ml, 60 μg/ml, and 120 μg/ml), different concentrations of S3I-201 (Selleck Chemical, Houston, TX, USA; 25 μM, 50 μM, 100 μM, and 200 μM), or the extracted liquids of PCL/PVA or PCL/Ade-$PVA_{(0.3/0.4)}$ membranes; BMMs (10^5 cells/well) were seeded in 96-well plates and were co-cultured with RANKL (PeproTech, USA; 50 ng/ml), M-CSF (PeproTech, USA; 50 ng/ml) combined with or without different concentrations of adenosine (15 μg/ml, 30 μg/ml, and 60 μg/ml). Medium was replaced with CCK8 solution at the harvest time (1^{st}, 3^{rd}, and 5^{th} days) and then incubated for 1.5 h at 37 °C, after which a microplate reader (Biotek, VT, USA) was used to generate the OD values with the absorbance recorded at a wavelength of 450 nm.

2.3. Alizarin red staining

Cells or nanofibrous membranes were washed twice with phosphate-buffered saline (PBS) and then were fixed in 4% formaldehyde for 15 min at room temperature. Then, the membranes were washed with PBS for three times, which was followed by the addition of 1% Alizarin red S staining solution (pH 4.2) and incubated for 30 min at 37 °C away from light. After subsequently rinsed three times with distilled water slightly, all the samples were prepared for microscopic observation. 10% cetylpyridinium chloride (Sigma-Aldrich, St.Louis, USA) was used to dissolve the calcium deposition for quantitative detection, which was determined by the OD value of collected solution measured at 562 nm.

2.4. RNA extraction and quantitative real-time PCR

RNA samples were isolated using an EZNA total RNA kit (Omega, Norcross, USA). Then Nanodrop2000 (Thermo Fisher Scientific, USA) was used to measure the concentration of the total RNA samples, which were used for the complementary DNA (cDNA) synthesis via Prime Script RT-PCR Kit (TaKaRa, Japan) according to the manufacturer's instructions. RT-qPCR was performed on a Bio-Rad CFX 96 real-time PCR machine by using the All-in-One™ qPCR Mix (GeneCopoeia, Rockville, USA) to analyze the expression levels of osteogenic and osteoclastogenic related genes relative to the mRNA expression levels of GAPDH with the $2^{-\Delta\Delta Ct}$ method. The primer sequences of target genes are listed in Table S1.

2.5. Western blot analysis

Cells were washed twice in PBS and then were lysed with radio immunoprecipitation assay (RIPA; Thermo Fisher Scientific, USA) buffer containing 1% phenylmethanesulfonyl fluoride (PMSF; Roche, Basel, Switzerland). After normalizing all the protein samples to 20 mg according to the measurement of protein concentration via a Pierce™ BCA Protein Assay Kit (Thermo Fisher Scientific, USA), proteins were separated by 10% SDS-PAGE gels and subsequently transferred to PVDF membranes (Roche, Basel, Switzerland). The membranes were blocked with 5% skim milk in TBST solution for 1 h at room temperature, and then incubated with primary antibodys against p-STAT3 (1:2000, CST, USA), STAT3 (1:2000, CST, USA), Osterix (1:2000, Abcam, UK), Alp (1:3000, Abcam, UK), Runx2 (1:1000, Abcam, UK), and GAPDH

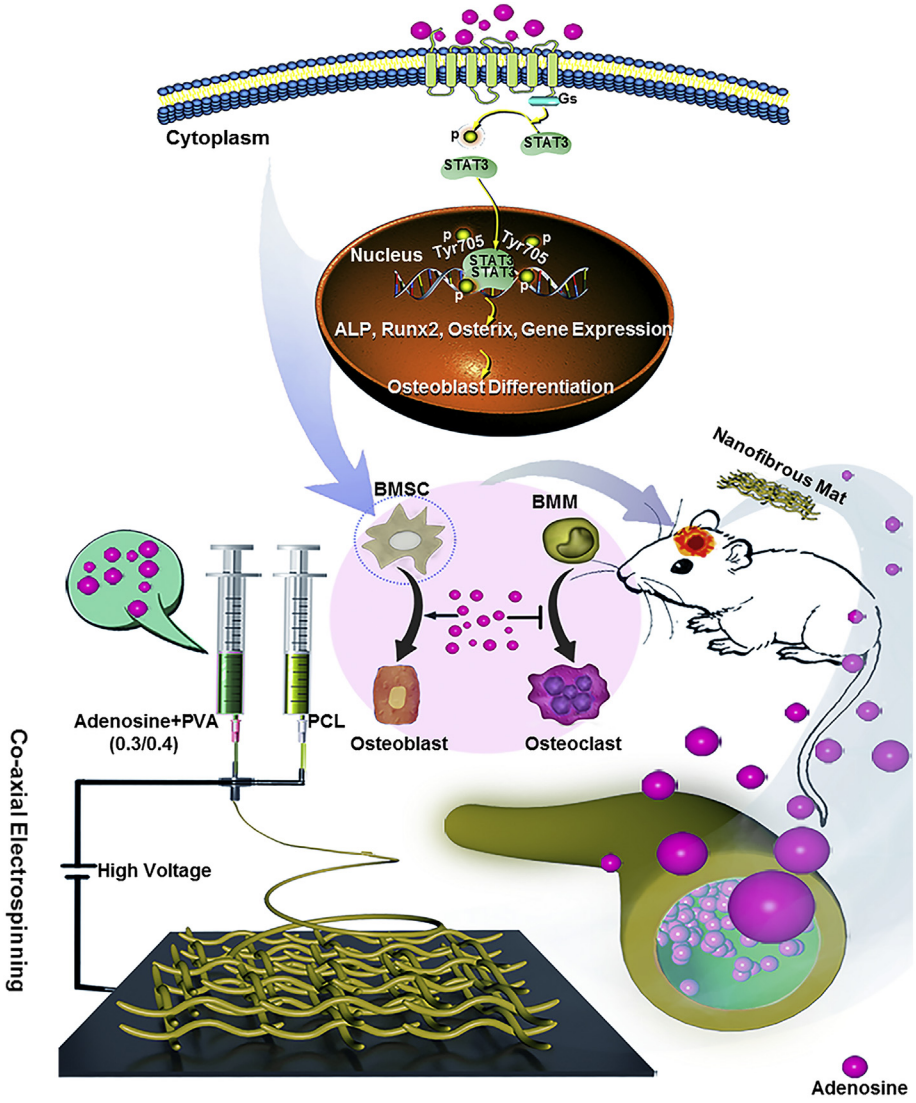

Scheme 1. Schematic illustration of application of PCL/Ade-PVA$_{(0.3/0.4)}$ nanofibrous mats to induce bone regeneration in a rat cranial defect model. The PCL/PVA nanofibers were assembled by coaxial electrospinning with adenosine incorporated in the core of the nanofibers. The adenosine that continuously released from the fibers with 0.3:0.4 (w/w) ratio of Ade and PVA could facilitate the defect healing through promotion of differentiation of BMSCs into osteoblasts via STAT3 signaling pathway and inhibition of differentiation of BMMs into osteoclasts.

(1:5000, Proteintech, USA) at 4 °C overnight. Thereafter, the membranes were incubated with HRP-conjugated secondary goat anti-rabbit IgG (1:10000, Abbkine, USA) or goat anti-mouse IgG (1:10000, Abbkine, USA) for 1 h at room temperature, after which the targeted protein bands were detected with the WesternBright ECL HRP substrate Kit (Advansta, USA).

2.6. Immunofluorescence staining

The adherent BMSCs were stimulated with dimethyl sulfoxide (DMSO; 100 μM, as vehicle control), adenosine (60 μg/ml) + DMSO (100 μM), or adenosine (60 μg/ml) + S3I-201 (100 μM) for 1 h, then were successively subjected to fixation with 4% paraformaldehyde for 15 min, permeabilization with 0.5% Triton X-100 for 15 min, and blockade with 1% bovine serum albumin for 1 h at 37 °C. Subsequently all the samples were incubated with primary antibody against p-STAT3 (1:250, CST, USA) at 4 °C overnight. After incubated with anti-rabbit secondary antibody with red fluorescent marker (1:500, Abbkine, USA) and counterstained of nuclei with DAPI, representative stained images were observed under an Olympus DP72 microscope (Tokyo, Japan).

2.7. Tartrate-resistant acid phosphatase (TRAP) staining

After being fixed with 4% paraformaldehyde for 15 min, the cells were incubated with TRAP solution using kit 387-A (Sigma-Aldrich, St.Louis, USA) following the manufacturer's instructions for 10 min at room temperature in the dark, which was followed by counterstain nuclei with DAPI (Beyotime, Hangzhou, China) for 5 min away from light. Finally, the samples were washed with PBS solution slightly and stored in PBS solution for further observation under light microscopy.

2.8. Preparation of PCL/Ade-PVA composite mats

PCL/Ade-PVA composite nanofibrous mats were fabricated through the co-axial electrospinning technology according to our previous study [31]. Briefly, the sheath solution (10% PCL, w/w) was firstly prepared by dissolving 10 g PCL (70,000–90,000 DA, Sigma-Aldrich, St.Louis, USA) in 100 g hexafluoroisopropanol (HFIP) (Aladdin Co., China). Then, the core solutions with 0.1/0.6, 0.2/0.5, 0.3/0.4 and 0.4/0.3 ratios of adenosine and PVA were made by dispersing 0.1, 0.2, 0.3, and 0.4 g adenosine in 10 ml PVA (85,000–14,000 DA, Sigma-Aldrich, St.Louis, USA) aqueous solutions containing 0.6, 0.5, 0.4, 0.3 g PVA,

respectively. After magnetic stirring for 2 h and ultra-sonication for 0.5 h in an ice bath, the adenosine-PVA solutions were used as a core-solution. 10 ml PVA solution without adenosine incorporation was used as the Empty control group. The co-axial electrospinning system was equipped with a metal collector, a high DC voltage of 20 kV, the inner and outer spinnerets. The sheath- and core-solution were transported into the outer and inner syringes, respectively. All the electrospinning processes were performed at 27 ˚C and 60% humidity.

To visualize the distribution of the adenosine-PVA solution in the composite nanofibers, 10 mg calcein and 10 mg rhodamine B were added into core- and sheath solution, respectively. Then, the calcein/Ade-PVA solutions with a green color and the rhodamine B/PCL solution with a red color were observed by confocal microscopy (LEICA SP8 STED, Germany).

2.9. Characterizations

The morphology of the PCL/Ade-PVA samples was observed by a scanning electron microscopy (SEM, ZEISSΣ SIGMA, Germany). The diameter of 100 different fibers per image was measured to determine the mean diameter of the PCL/Ade-PVA composite mats using Nano-measurer 1.2 software. The dynamic water contact angles (WCA) of the PCL/Ade-PVA composite nanofibrous mats were evaluated by the drop shape analysis equipment (USA KINO Industry Co., USA). The stress–-strain responses of the PCL/Ade-PVA composite mats were analyzed by an ETM502A tensile tester (Shenzhen Wance Instrument Co., Ltd., China) after all the samples were cut into 3 × 1 cm. The cytocompatibility of the prepared composite mats was determined by fluorescent Live/Dead staining using a LIVE/DEAD™ Cell Imaging Kit (Thermo Fisher Scientific, USA) and then observations under a confocal laser scanning microscope (Olympus, Tokyo, Japan) after cultured with the seeding BMSCs for 3 days.

2.10. High-performance liquid chromatography (HPLC) analysis of released adenosine content

Five replicates of the round PCL/Ade-PVA$_{(0.3/0.4)}$ composite nanofibrous mats (diameter = 5 mm), which were as same as that used in animal experiments, were incubated in 3 ml distilled water in a 37 ˚C water bath with slow shake for 1, 15, 30, 45, and 60 days. At each time interval, the extract liquid was removed with fresh water replaced, and 1 ml was used for HPLC analysis using an Agilent 1200 HPLC System combined with a Hisep C18 column (4.6 × 250 mm, 5 μm, Weltech, Wuhan, China). Samples were eluted by the mobile phase that consisted of 10 mmol/L potassium dihydrogen phosphate and methyl alcohol in a volume ratio of 85:15, with a 0.9 ml/min flow rate and a detection wavelength of 257 nm at 35 ˚C. Commercial adenosine standard (Sigma-Aldrich, St.Louis, USA) of five different concentrations (600, 300, 150, 75, and 35.5 μg/ml) were analyzed as control and used to plot the standard curve. The run time for the adenosine retention was 20 min.

2.11. In vivo cranial defect study

The protocols of this study were approved by the Ethics Committee of School and Hospital of Stomatology, Wuhan University (Accreditation number was 00273633). Thirty SD rats (male, 6 weeks old, 200–250 g) were housed under specific pathogen free condition and received calvarial defect surgery under anesthesia in a sterile environment. Briefly, two full- thickness circular bone defects (diameter = 5 mm) were created on both sides of the skull while irrigating with saline solution. Then all the rats randomly fell into three groups (ten rats per group) according to various nanofibrous membranes for bone defects implantation: sham + PCL/PVA (additionally intraperitoneal injection of DMSO every 2 days as vehicle control, 10 mg/kg); PCL/PVA + PCL/Ade-PVA$_{(0.3/0.4)}$ (additionally intraperitoneal injection of DMSO every 2 days as vehicle control, 10 mg/kg); PCL/PVA + PCL/Ade-PVA$_{(0.3/0.4)}$ + S3I-201 (intraperitoneal injection every 2 days, 10 mg/kg).

2.12. Micro-computed tomography (micro-CT) measurement and histological analysis

The nanofibrous membrane-covered craniums were collected at 4 weeks or 8 weeks post implantation. Bone regeneration in the calvarial defects was evaluated using a micro-CT system (SkyScan 1176, Belgium) at a resolution of 20 μm. Then three-dimensional reconstructed images were created by using CTvox software, meanwhile the new bone volume over total bone volume (BV/TV) and the percentages of bone mineral density (BMD) were measured.

For histological analysis, at harvest time points, the specimens were fixed with 4% paraformaldehyde for 24 h at 4 ˚C before decalcified in 10% EDTA solution at room temperature for 4 weeks. Then the decalcified samples were carefully trimmed and subjected to 70%, 80%, 90%, 95%, and 100% ethyl alcohol in a gradient sequence for dehydration and subsequently embedded in paraffin blocks. The embedded samples were sectioned 5 mm thick from the center of the repair site and stained with haematoxylin-eosin (HE) staining, Masson's trichrome staining and immunohistochemistry staining. For immunohistochemistry staining, the primary antibody against Col1 (1:500; Abcam, UK) was used and the expression of Col1 in the defect site areas was visualized by 3, 3-diaminobenzidine tetrahydrochloride (DAB) (Zhongshan Biotechnology, Ltd., China). Lastly, the images of all the stained slices were observed and captured using an optical microscope (Olympus DP72, Tokyo, Japan).

2.13. Statistical analysis

All experiments were repeated independently at least six times with results analyzed via GraphPad Prism software 3.06 and reported as mean and standard deviation. Statistical evaluation was performed through Two-way ANOVA and Students'*t*-test. Values of $P < .05$ were considered significantly different.

3. Results and discussion

3.1. Influence of adenosine on the osteogenic differentiation of BMSCs

To evaluate the effect of adenosine on the osteogenesis of BMSCs *in vitro*, Alizarin Red staining was performed to observe the deposition of calcium nodules after treatment with the growth medium supplemented with different concentrations of adenosine (Fig. S1A, B). Similar to the results in a previous study, in which adenosine can solely drive the differentiation of human induced pluripotent stem cells (hPSCs) into osteoblasts [32], we verified that 60 μg/ml adenosine can significantly enhance the formation of mineralized nodules compared with the lower concentration groups (15 μg/ml and 30 μg/ml, $p < .05$). However, no significant difference was observed between the 60 μg/ml adenosine group and conventional mineralized induction medium group ($p > .05$). In our study, at higher concentration of adenosine (120 μg/ml), the osteogenic efficacy became lower. This phenomenon may be explained by the fact that the influence of excessive exogenous adenosine on osteogenic differentiation may be restricted because of the enzymolysis of adenosine mediated by ecto-ADA and ADK [6,8]. Another possible explanation is that high adenosine levels can lower the sensitivity and specificity of relevant adenosine receptors participating in the modulation of osteoblast function [33]. To evaluate the cytotoxicity of adenosine, CCK8 assay was performed to test the viability of the BMSCs after treatment with 15, 30, 60, or 120 μg/ml of adenosine. No significant differences were detected among the groups ($p > .05$) (Fig. S1C), suggesting that exogenous adenosine had no significant cytotoxic effects on the BMSCs.

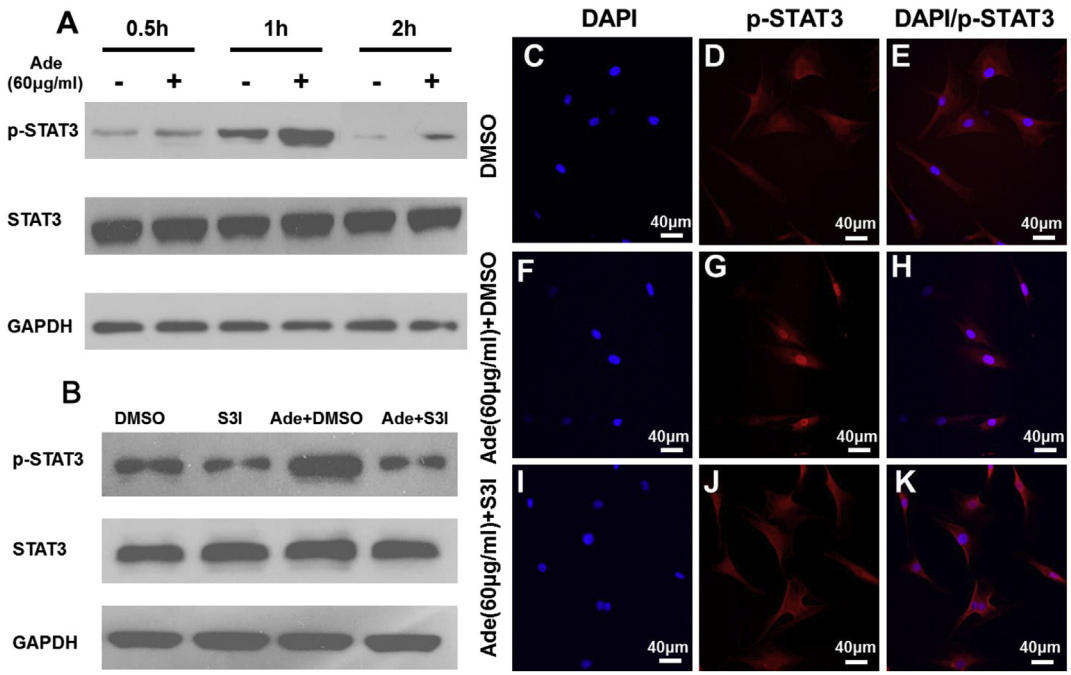

Fig. 1. Adenosine promoted STAT3-mediated osteogenesis of BMSCs.
BMSCs were treated with the indicated concentrations of adenosine for 0.5, 1, and 2 h (A), or DMSO (100 μM), SCI-201 (100 μM), adenosine (60 μg/ml) combined with DMSO (100 μM), and adenosine (60 μg/ml) combined with SCI-201 (100 μM) for 1 h (B), Western blot detected the protein levels of p-STAT3, STAT3, and GAPDH. After treatment with DMSO (100 μM), adenosine (60 μg/ml) combined with DMSO (100 μM), and adenosine (60 μg/ml) combined with SCI-201 (100 μM) for 1 h, representative immunofluorescent photos displayed the nuclear levels of STAT3 (red) (C–K). Ade, adenosine. S3I, S3I-201. (For interpretation of the references to color in this figure legend, the reader is referred to the web version of this article.)

3.2. Participation of STAT3 signaling in the adenosine-mediated osteogenesis in BMSCs

Prior studies have shown the importance of STAT3, which was originally defined as a cytoplasmic transcription factor and further identified to play pivotal roles in different tissues, particularly in the bone [34]. In our previous study, we have also shown that blockade of JAK2/STAT3 signaling by AG490, a selective JAK2 inhibitor, results in the suppression of hypoxia-induced osteogenesis of BMSCs and bone defect healing [35]. Given that almost all STAT genes and proteins are expressed in the osteoblasts, in the present study, we determined the role of STAT3 in adenosine-mediated osteogenesis of BMSCs. As shown in Fig. 1A, the Western blot results revealed that STAT3 was activated by adenosine (60 μg/ml) at a rapid time within 0.5 h. Furthermore, the phosphorylation level significantly augmented the expression at 1 h and then lasted for 2 h. We did not observe any evidence that adenosine had an influence on JAK2 phosphorylation (data are not shown). Therefore, we considered S3I-201, a selective STAT3 inhibitor. We incubated BMSCs with different concentrations of S3I-201 (25, 50, 100, and 200 μM) and found that 200 μM S3I-201 exerted evident cytotoxicity, resulting in reduced cell proliferation (Fig. S2). Moreover, we chose 100 μM as the experimental concentration. The results showed that 100 μM S3I-201 can remarkably downregulate adenosine-induced phosphorylation of STAT3 (p-STAT3) in the protein level (Fig. 1B) and reversed adenosine-induced nuclear translocation of STAT3 in the BMSCs (Fig. 1C–K). Alizarin Red staining was used to evaluate the effect of S3I-201 on the adenosine-induced osteogenic differentiation of BMSCs. Similar to the decreased calcification in the conventional mineralized medium group after the treatment of S3I-201, the addition of S3I-201 can significantly prevent the calcium deposition induced by adenosine (Fig. 2A–F and Fig. S3). These results indicated that STAT3 signaling was involved in the adenosine-induced osteogenesis of BMSCs. Moreover, the effect of adenosine on this osteogenesis was further evaluated through real-time PCR. Adenosine enhanced the RNA expression of the osteoblast-specific markers ALP, Col1, Osterix, and Runx2, and these effects can be inhibited by S3I-201 (Fig. 2G–J, $p < .05$). The expression of these proteins showed the same tendency with the gene expression profile (Fig. 2K). Previous studies have mostly focused on the adenosine receptors when the potential mechanisms in the osteoblast metabolism were considered. A2AR acted as a medium for adenosine to accelerate the proliferation of mouse BMSCs [36]. During the osteoblast differentiation of the BMSCs, the A2AR signal was enlarged to facilitate the alkaline phosphatase activity [37]. A2BR KO mice showed a reduction in the osteoblast differentiation, osteoblast-related gene expression, and calcium deposition in the mesenchymal cells [38]. By contrast, our study demonstrated a possible downstream signal transduction mechanism of adenosine in osteogenesis, which depended on the activation of STAT3 signaling.

3.3. Effect of adenosine on osteoclast precursors

The maintenance of bone tissue homeostasis depends on the favorable skeleton turnover, including the bone formation and bone resorption mediated by osteoblasts and osteoclasts, respectively. With unique and impressive morphology, a mature osteoclast is a kind of multinuclear macrophage [39] and positively expresses tartrate-resistant acid phosphatase (TRAP). Therefore, we performed TRAP staining to evaluate the effect of adenosine on the osteoclast differentiation of rat bone-marrow macrophages (BMMs), which was induced by macrophage colony stimulating factor and receptor activator of nuclear factor (NF)-κB ligand (Fig. 3A–D). As shown in the Figs. 3, 15 or 30 μg/ml adenosine did not affect the formation of TRAP-positive multinucleated cells (Fig. 3A–C). By contrast, 60 μg/ml adenosine obviously diminished the osteoclastic differentiation of BMMs (Fig. 3D), resulting in the distinct reduction in the mature osteoclasts (Fig. 3E, $p < .05$). Meanwhile, 60 μg/ml adenosine promoted cell proliferation at 3 and 5 days (Fig. 3F, $p < .05$). These results indicated that 60 μg/ml adenosine may inhibit osteoclastic differentiation while promoting the

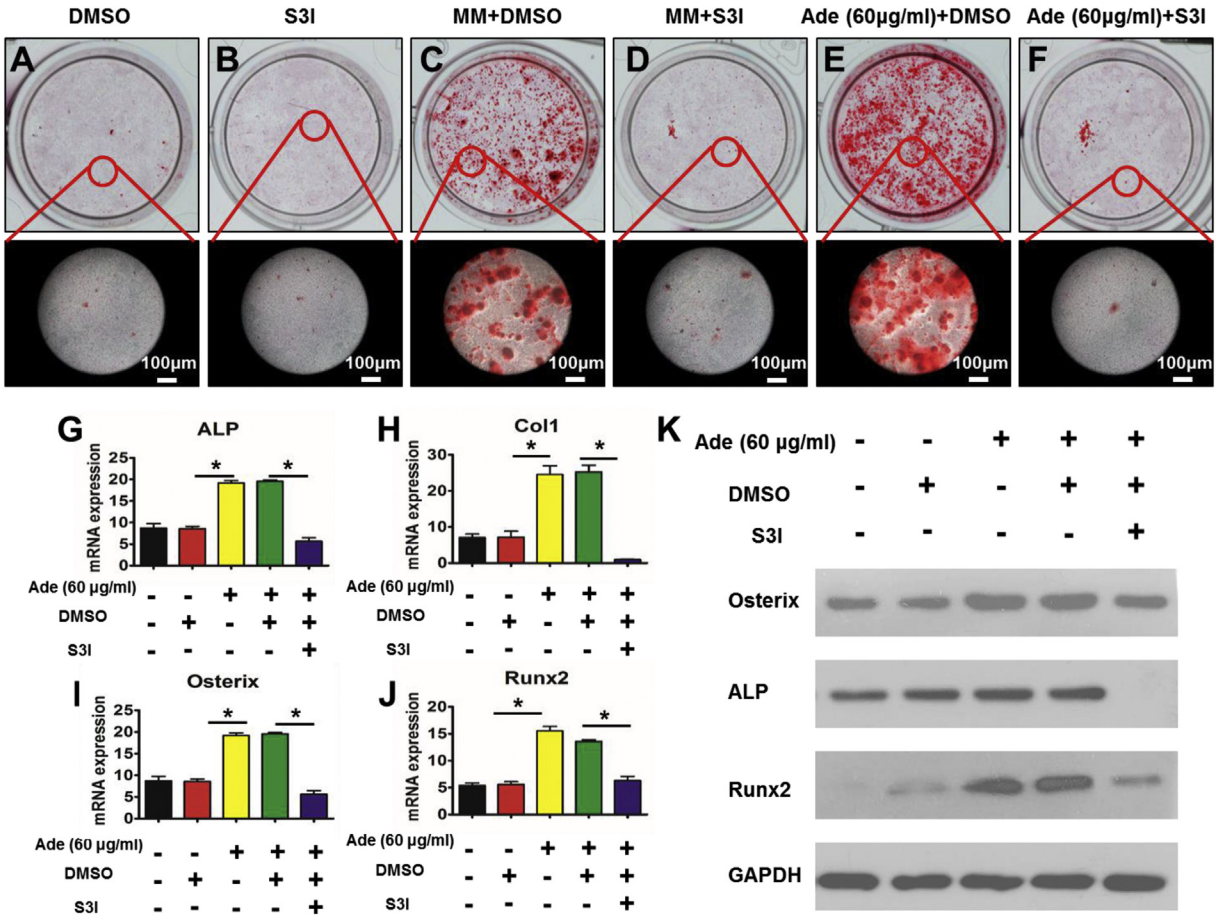

Fig. 2. SCI-201 inhibited adenosine-induced osteogenesis.
Representative macroscopic and microscopic images of Alizarin Red staining for evaluation of the osteogenesis induced by respective groups for 21 days in BMSCs (A–F). Real-time PCR and Western blot analysis further revealed that SCI-201 (100 μM) not only inhibited osteoblast-related genes ALP, Col1, Osterix, and Runx2 mRNA levels (G–J), but also suppressed their protein levels induced by adenosine (60 μg/ml) in BMSCs (K). S3I, S3I-201. MM, mineralized medium. Ade, adenosine. *$P < .05$. The Students' *t*-test.

proliferation of osteoclast precursors. These results provide a new understanding of the mechanism of adenosine during bone healing and establish a foundation for the further development of clinical treatment using adenosine.

3.4. Characteristic of the PCL/adenosine-PVA nanofibrous mats

Considering that the promotion of adenosine on the osteogenesis of BMSCs is dose-dependent, and high concentration of adenosine has restricted this osteogenesis, we fabricated a coaxial nanofibrous mat for the controlled release of adenosine with appropriate concentrations to promote new bone formation.

The morphology of the fabricated PCL/Ade-PVA composite nanofibrous mats was characterized by a scanning electron microscope (SEM). Fig. 4 shows that the PCL/Ade-PVA composite nanofibrous mats had highly porous 3D net-like structures (Fig. 4A–D). The PCL/PVA nanofibrous mat without adenosine showed a nonuniform diameter distribution (Fig. 4E, 735 ± 610 nm). With the incorporation of adenosine, the diameters of PCL/Ade-PVA$_{(0.1/0.6)}$ (Fig. 4A, 1019 ± 535 nm), PCL/Ade-PVA$_{(0.2/0.5)}$ (Fig. 4B, 1424 ± 731 nm), PCL/Ade-PVA$_{(0.3/0.4)}$ (Fig. 4C, 1398 ± 280 nm), and PCL/Ade-PVA$_{(0.4/0.3)}$ (Fig. 4D, 2019 ± 1052 nm) nanofibers showed a more uniform distribution compared with that of the PCL/PVA group. Among all groups, the PCL/Ade-PVA$_{(0.3/0.4)}$ composite nanofibrous mat exhibited the most uniform distribution of fiber diameter (Fig. 4F–J). This result suggested that the most suitable ratio of adenosine to PVA was 0.3:0.4. Therefore, the PCL/Ade-PVA$_{(0.3/0.4)}$ composite nanofibrous mat was used in the following experiments.

The stress–strain curves (Fig. 5A) show that the PCL/PVA composite nanofibrous mats were broken at 3.52 ± 0.56 Mpa when the elongation reached approximately 155.41% ± 43.24%. With the incorporation of adenosine, the elongation at break of the PCL/Ade-PVA$_{(0.3/0.4)}$ composite nanofibrous mats did not remarkably change (124.93% ± 29.23%, $p > .05$). However, the stress at break of the PCL/Ade-PVA$_{(0.3/0.4)}$ group significantly increased and reached 7.1 ± 1.33 Mpa ($p < .05$). These results indicated that adenosine incorporation improved the mechanical properties of the PCL/PVA coaxial nanofibrous mats. As shown in Fig. 5B, the water contact angles (WCAs) of the PCL/PVA composite mats were 87.5° ± 8.36°, 71.5° ± 8.36°, and 30.28° ± 8.36° at 20, 60, and 100 s, respectively. With the incorporation of adenosine, the WCAs of the PCL/Ade-PVA$_{(0.3/0.4)}$ composite nanofibrous mats were decreased to 73.5° ± 8.36°, 68.5° ± 6.36°, and 17.28° ± 3.36° at 20, 60, and 100 s, respectively. Slightly longer time was observed for the PCL/Ade-PVA$_{(0.3/0.4)}$ nanofibrous mats (118 s) to completely absorb the water droplets compared with that of the PCL/PVA mats (108 s, Fig. S4A). However, this discrepancy had no significant statistical difference (Fig. S4B, $p > .05$). These results demonstrated that adenosine incorporation had little influence on the hydrophilicity of the PCL/Ade-PVA$_{(0.3/0.4)}$ nanofibrous mats. Confocal microscopy was used to observe the core–sheath structure of the co-axial PCL/Ade-PVA nanofibers. As shown in Fig. 5D, the PVA or Ade-PVA core with a green color was uniformly distributed at

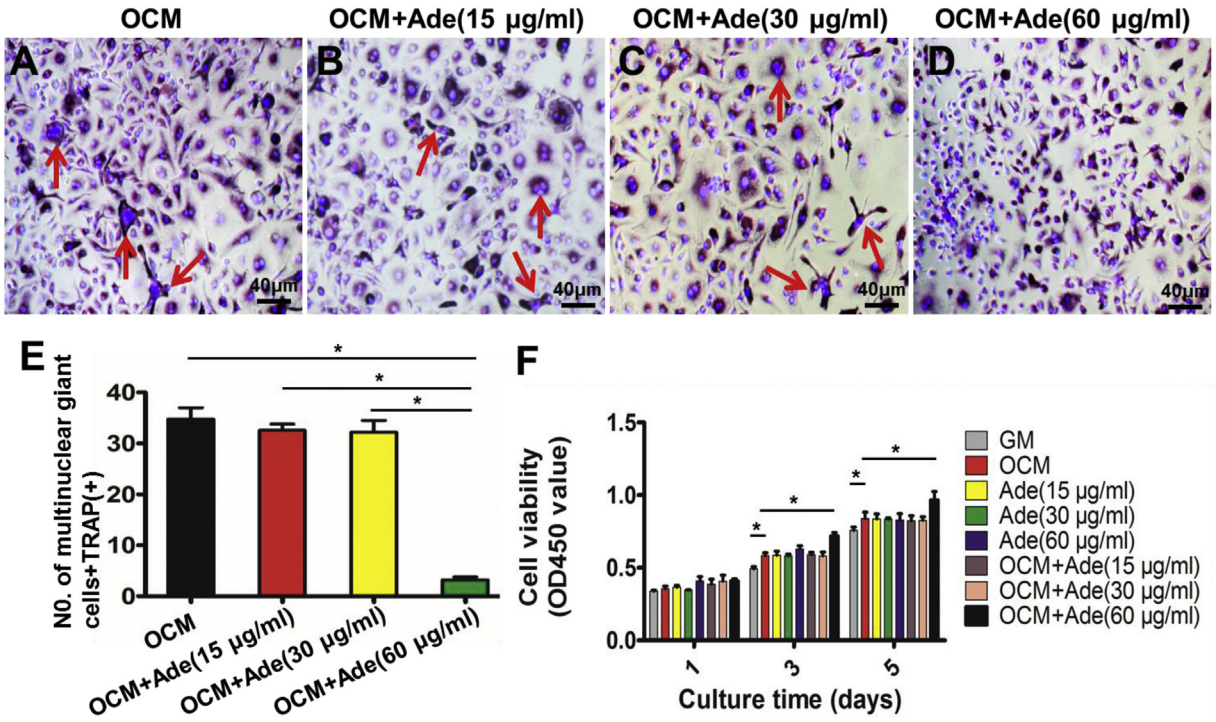

Fig. 3. High concentration of adenosine suppressed osteoclastogenesis of BMMs.
TRAP staining was used to evaluate osteoclastic differentiation of BMMs (A–D) at 8 days of induction. 60 μg/ml adenosine reduced mature osteoclasts formation (highlighted by the red color arrow) (D, E), while promoted the proliferation of BMMs detected by CCK-8 assay (F). OCM, osteoclast differentiation medium. Ade, adenosine. *P < .05. The Students' t-test. (For interpretation of the references to color in this figure legend, the reader is referred to the web version of this article.)

the center of the PCL/PVA and PCL/Ade-PVA$_{(0.3/0.4)}$ nanofibers with red color. The cytocompatibility of the PCL/Ade-PVA nanofibrous mats was evaluated by Live/Dead staining. From the results in Fig. 5E and the negative and positive controls exhibited in Fig. S5, BMSCs seeded onto the PCL/PVA and PCL/Ade-PVA$_{(0.3/0.4)}$ nanofibrous mats exhibited a green color. The CCK-8 assay showed that the extract liquid from both nanofibrous mats exhibited no evident cytotoxicity to reduce cell activities in BMSCs (Fig. S6). Thus, these results demonstrated that the PCL/PVA and PCL/Ade-PVA$_{(0.3/0.4)}$ nanofibrous mats were not cytotoxic to the BMSCs. The morphology of the BMSCs seeded onto the PCL/PVA and PCL/Ade-PVA$_{(0.3/0.4)}$ (Fig. 5F) nanofibrous mats was examined by an SEM. The cells on the PCL/PVA nanofibrous mat were spindle shaped, contrary to the polygon-shaped cells on the PCL/Ade-PVA$_{(0.3/0.4)}$ nanofibrous mat. These results demonstrated that adenosine might promote the stretching of cells.

3.5. Drug release of adenosine-loaded PCL/PVA co-axial nanofibrous mats in vitro

To determine the drug releasing effect of the fabricated PCL/Ade-PVA$_{(0.3/0.4)}$ nanofibrous membranes, the extract liquid of the membranes at various time intervals (1, 15, 30, 45, and 60 days) was collected and then applied to HPLC assay. Representative chromatograms of adenosine retention are shown in Fig. S7. The samples (Fig. S7B–F) showed similar peak eluting time of ~12.4 min to the adenosine standard (150 μg/ml) (Fig. S7A), indicating that we have successfully

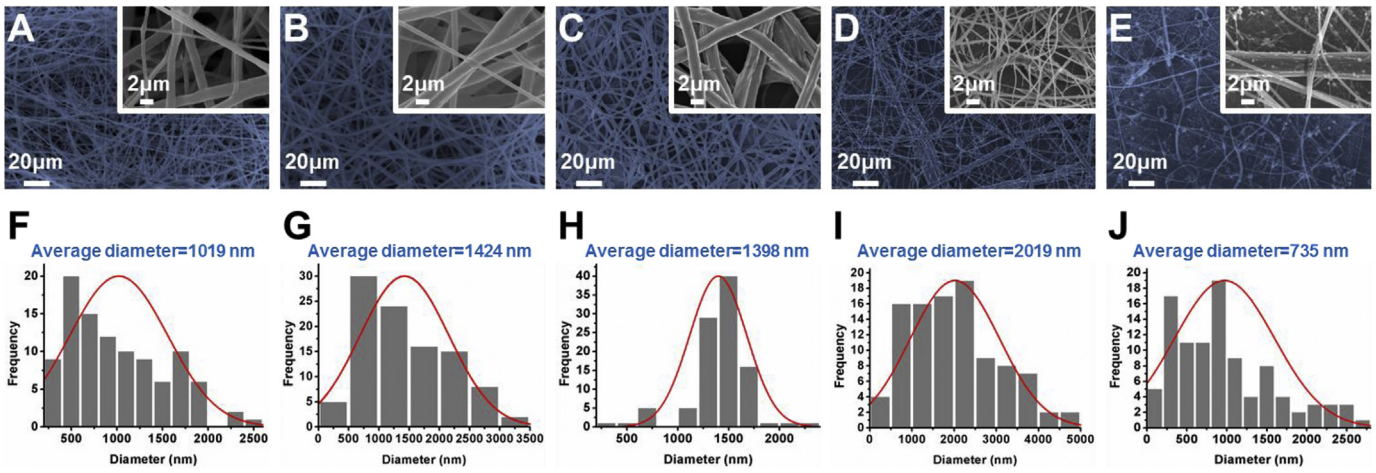

Fig. 4. SEM images of the nanofibrous membranes with different ratios of Ade and PVA. Representative images of PCL/Ade-PVA$_{(0.1/0.6)}$ (A), PCL/Ade-PVA$_{(0.2/0.5)}$ (B), PCL/Ade-PVA$_{(0.3/0.4)}$ (C), PCL/Ade-PVA$_{(0.4/0.3)}$ (D) and PCL/PVA (E) nanofibrous membranes, and their fiber diameter distributions, respectively (F–J). The nanofibers of the PCL/Ade-PVA$_{(0.3/0.4)}$ group is more uniform than those of the other groups. Data are presented as the mean ± SD. Ade, adenosine.

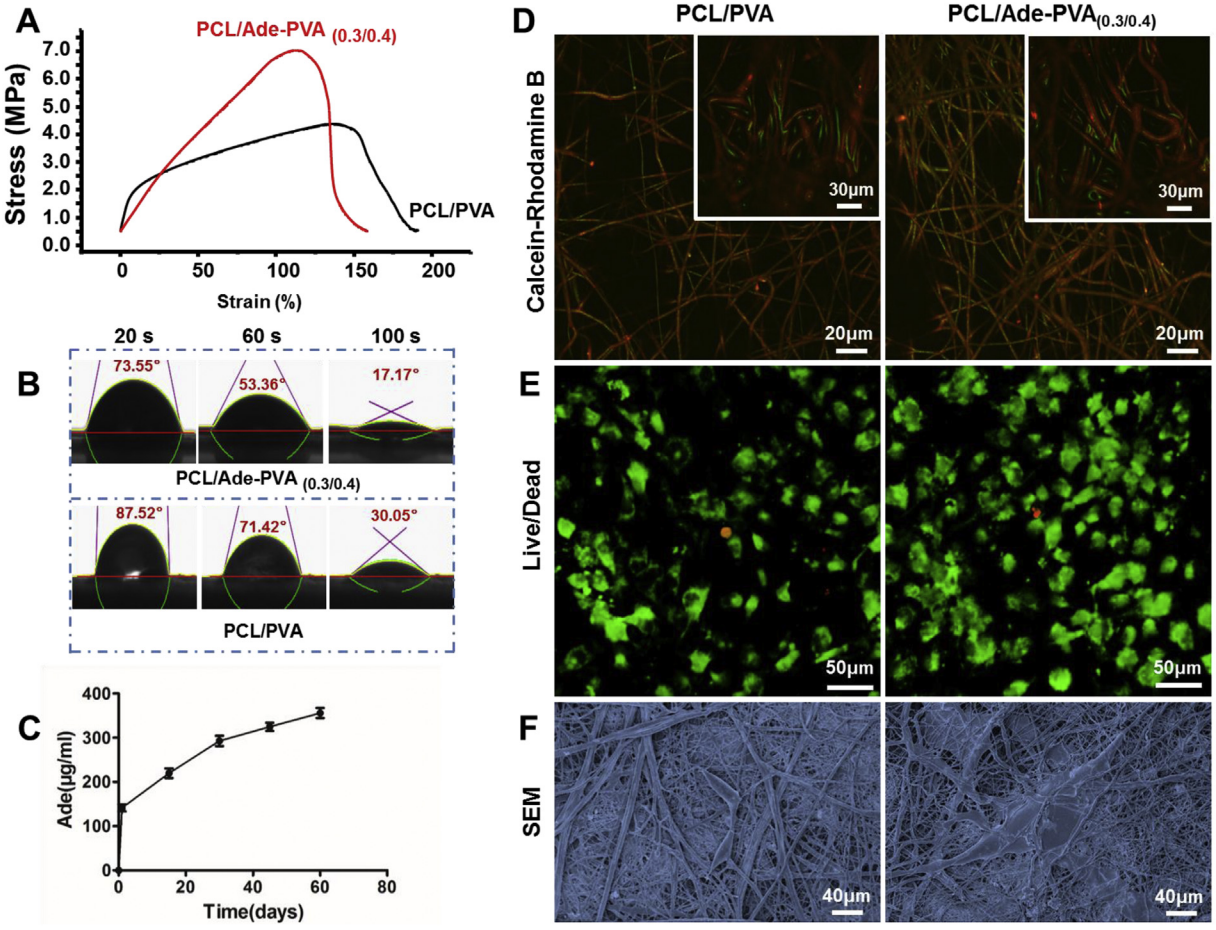

Fig. 5. Characterization of the co-axial nanofibrous membranes.
Typical stress–strain curves of the PCL/Ade-PVA$_{(0.3/0.4)}$ and PCL/PVA nanofibrous membranes (A).Water contact angles of the PCL/Ade-PVA$_{(0.3/0.4)}$ and PCL/PVA nanofibrous membranes (B). *In vitro* release kinetics of adenosine from the PCL/Ade-PVA$_{(0.3/0.4)}$ nanofibrous membrane as determined by high-performance liquid chromatography (C). Confocal images of the co-axial PCL/PVA and PCL/Ade-PVA$_{(0.3/0.4)}$ (D) nanofibers with the PVA or Ade-PVA core stained with calcein and the PCL sheath stained with rhodamine B. Confocal images of the PCL/PVA and PCL/Ade-PVA$_{(0.3/0.4)}$ (E) nanofibers with Live/Dead staining, and SEM images of the PCL/PVA and PCL/Ade-PVA$_{(0.3/0.4)}$ (F) nanofibers after BMSCs seeded for 3 days. Ade, adenosine.

achieved the sustained and controlled diffusion of adenosine from the PCL/Ade-PVA$_{(0.3/0.4)}$ nanofibrous mats for up to 60 days. Similar to a silk-based adenosine delivery system with sustained release of adenosine due to the degradation of the coated silk [40] and to the core-shell gel beads with the hydrophobic polymer coating that increased the release time of proteins [41], the slow release in this study can be attributed to the slow degradation of hydrophobic PCL. The quantification of the adenosine release from the nanofibrous mats is shown in Fig. 5C. Similar to other typical release profiles of layer-by-layer drug-delivery systems [42,43], an initial burst release of adenosine was observed in the PCL/Ade-PVA$_{(0.3/0.4)}$ nanofibrous mats on day 1, during which the concentration of the released adenosine was 146.37 ± 11.18 μg/ml. This phenomenon may be due to the fact that the adenosine on the fiber surfaces quickly diffused after the water infiltration [10]. Afterward, the release rate of adenosine became stable as PCL protected adenosine in the core from being released into the outer environment. With the slow degradation of the shell of PCL and the gradual exposure of water-soluble PVA, the encapsulated adenosine was continuously released, sustaining a linear release profile. The cumulative release concentrations on days 15, 30, 45, and 60 were 224.48 ± 14.45, 296.02 ± 17.05, 326.67 ± 11.30, and 359.31 ± 15.23 μg/ml, respectively (Fig. 5C). During the drug controlled-release phase, the cumulative release concentration at each time interval was within the effective range of concentration as confirmed by the results of previous *in vitro* experiments (Fig. S1). These results not only indicated that the PCL/PVA coaxial drug release system showed the characteristic biphasic behavior that performed a relatively constant release after an initial burst release [44,45] but also provided the foundation for application of the PCL/Ade-PVA$_{(0.3/0.4)}$ nanofibrous mats in the following animal study.

3.6. *In vivo* bone formation of calvarial defects

To further explore the effects of PCL/Ade-PVA$_{(0.3/0.4)}$ composite nanofibrous membranes on the repair of bone defect, SD rat cranial bone defects were first established and implanted with the PCL/PVA and PCL/Ade-PVA$_{(0.3/0.4)}$ nanofibrous membranes. Micro-CT was used to analyze the new bone formation after 4 and 8 weeks of healing. As shown in Fig. 6A–J, a small amount of bone was formed on the boundary of the bone cavity in the sham groups after 4 and 8 weeks (Fig. 6A, F), whereas PCL/PVA groups showed more calcific deposition (Fig. 6B, G). These results suggested that the non-loaded PCL/PVA nanofibrous membrane can induce osteogenesis to a certain degree. The largest amount of newly-formed bone was observed in the defect size covered by the modified PCL/PVA membranes incorporated with adenosine in the PCL/Ade-PVA$_{(0.3/0.4)}$ group (Fig. 6D, I). In terms of the PCL/Ade-PVA$_{(0.3/0.4)}$ membranes that were intraperitoneally injected with S3I-201 at a dose of 10 mg/kg every two days, the osteogenesis effect at the defect site of the PCL/Ade-PVA$_{(0.3/0.4)}$ groups was remarkably suppressed at both 4 and 8 weeks post-implantation (Fig. 6E,

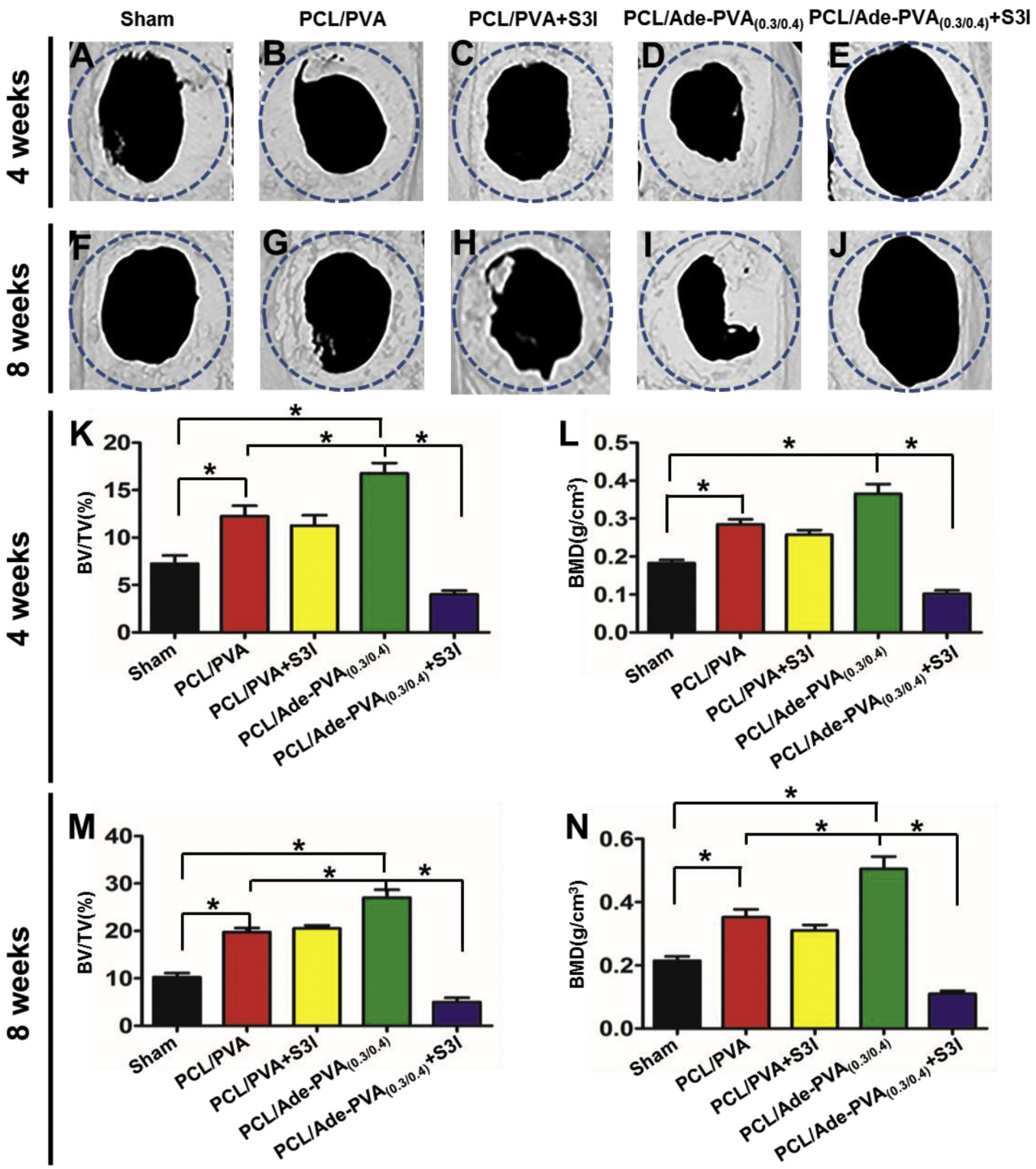

Fig. 6. The effects of fabricated nanofibrous membranes on new bone formation in the cranial defect model of SD rats.
Micro-CT images of bone formation in sham group (A, F), the implantation of PCL/PVA nanofibrous membranes (B, G) with intraperitoneal administration of SCI-201 (10 mg/kg) every two days (C, H), the implantation of PCL/Ade-PVA$_{(0.3/0.4)}$ nanofibrous membranes (D, I) with intraperitoneal administration of SCI-201 (10 mg/kg) every two days (E, J) at both 4 and 8 weeks. Quantification of the bone formation from the micro-CT images (K–N). S3I, S3I-201. Ade, adenosine. *P < .05. The Students' t-test.

J). However, S31–201 treatment showed little effect on the bone formation of the bare PCL/PVA group (Fig. 6C, H). The quantification of the bone mineral density and the percentage of BV/TV further confirmed that, although the PCL/PVA groups showed more bone regeneration than the sham groups, PCL/Ade-PVA$_{(0.3/0.4)}$ groups exhibited the most robust osteogenic efficacy, which could be reversed by the intraperitoneal administration of S3I-201 at 4 and 8 weeks (Fig. 6K–N, $p < .05$).

Histology assays, including HE, Masson trichrome staining, and immunohistochemical staining, of type I collagen (Col1) protein were further adopted to confirm the new bone formation and evaluate the newly formed bone morphology as shown in Fig. 7A–D and Fig. S8. 90% of the bone matrix is comprised of Col1 during the bone development, which could promote adherence and stimulate osteogenic differentiation of mesenchymal stem cells [46]. Moreover, Col1 is functionalized mainly during the early stages of bone healing to induce

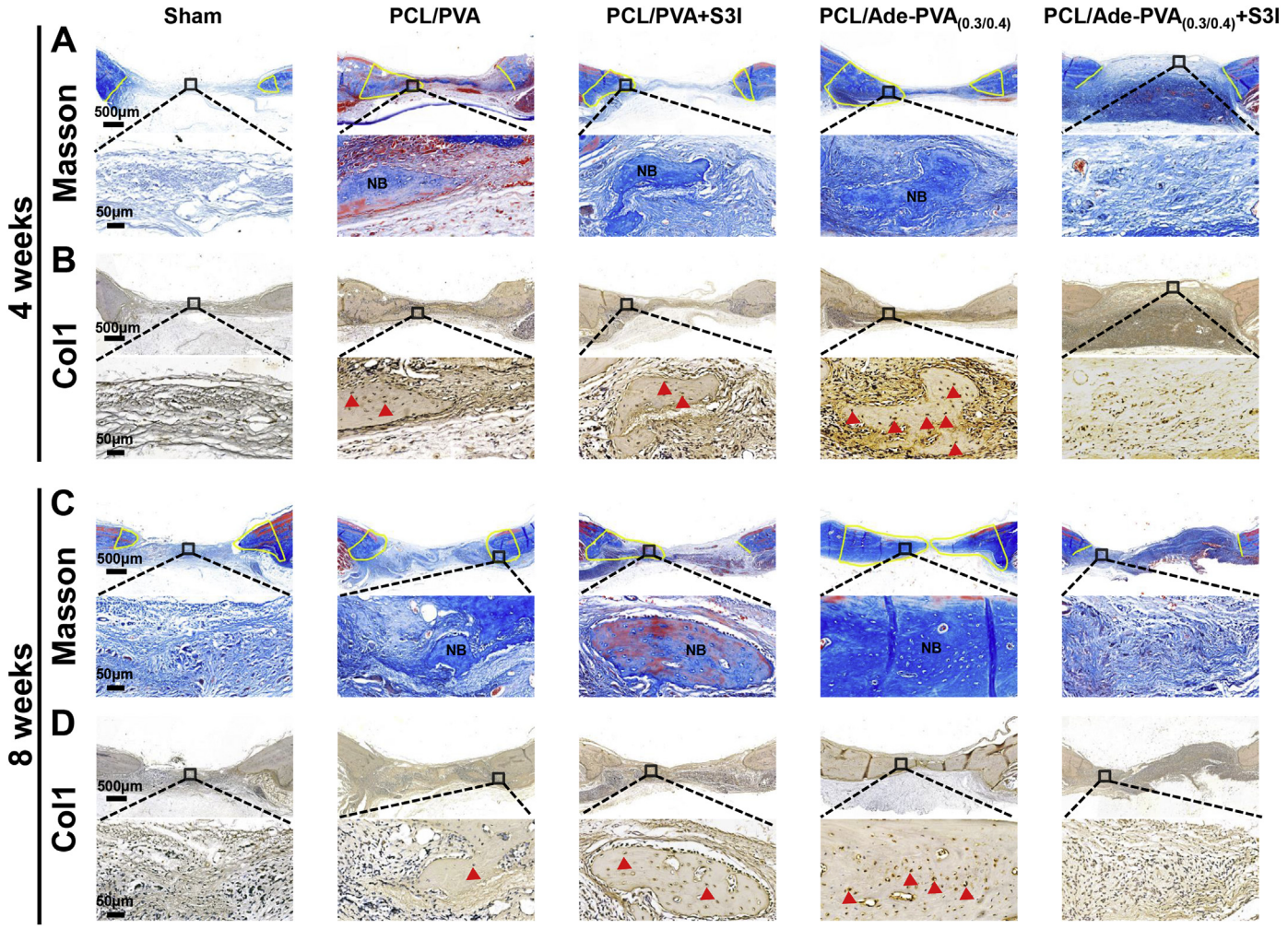

Fig. 7. Histological evaluation of newly formed bone.
Representative images showing masson trichrome staining (A, C; newly formed bone is outlined by a yellow line; NB: new bone), and immunohistochemical staining of the Col1-positive cells (B, D; labeled by red triangles) in the defect areas at 4 and 8 weeks. (For interpretation of the references to color in this figure legend, the reader is referred to the web version of this article.)

osteoblastic differentiation and form mineralized bone tissues [47]. In our current study as shown in Fig. 7B, D, both at 4 and 8 weeks post-implantation, the PCL/PVA group showed elevated Col1-positive areas compared with the sham group, but no significant difference was found compared with that of the PCL/PVA group combined with S3I-201 administration. This result suggested that STAT3 signaling may not be involved in the bone regeneration induced by the PCL/PVA membranes. Moreover, higher Col1 expression level was found within the defect regions in the PCL/Ade-PVA$_{(0.3/0.4)}$ group than that of the pure PCL/PVA group, but the intervention by S3I-201 led to reduced Col1 expression (Fig. 7B, D). These results indicated that the contribution of PCL/Ade-PVA$_{(0.3/0.4)}$ nanofibrous membranes to osteogenesis in bone defects may be primarily related to the release of adenosine that activated the STAT3 signaling. These results also agreed with those of Alizarin Red staining of BMSCs cultured with the PCL/Ade-PVA$_{(0.3/0.4)}$ nanofibrous membranes *in vitro* (Fig. S9).

To evaluate the possible side effects brought by adenosine application, the hemodynamics and serum functional biomarkers of animals in all groups were evaluated after creation of cranial defects and intravenous injection of adenosine or 0.9% saline solutions. Although adenosine was commonly used to treat the patients with myocardial infarct in large-scale clinical trials [48,49], this agent caused unfavorable hemodynamic effects, such as hypotension and bradycardia [50]. Therefore, it is necessary to release adenosine into the physiological environment in a controlled rate for minimizing the adverse side effects of systemic administration. As shown in Fig. S10, the intravenous injection of adenosine resulted in the decrease of the mean blood pressure and heart rate at the first 10 min of injection ($p < .05$) and sustained for another 5 min when compared with that of the sham group, which is conformed with the results of the previous study that intravenous injection of adenosine decreased blood pressure and heart rate [7]. No significant difference in mean blood pressure or heart rate was observed among the control, sham, PCL/PVA, PCL/PVA + S3I and PCL/Ade-PVA$_{(0.3/0.4)}$, PCL/Ade-PVA$_{(0.3/0.4)}$ + S3I groups ($p > .05$). In addition, the activity of alanine aminotransferase (ALT) and aspartate transaminase (AST) enzymes were tested on day 7, 14, and 21 after surgery (Table S2) to examine the hepatotoxicity in consideration of the fact that ADK exists in liver with a highest level, and the ADK-mediated phosphorylation of adenosine is believed to be one of the primary route of adenosine metabolism [51]. However, no significant difference was found among all groups during the whole time period ($p > .05$), which indicated that neither intravenous injection nor controlled release of adenosine led to the obvious hepatotoxicity. Therefore, the above mentioned results suggested that our fabricated core-shell nanofibers for adenosine delivery could significantly reduce the undesirable hypotension and bradycardia induced by systemic administration.

4. Conclusions

In summary, we developed a novel drug-delivery system for adenosine by using PCL/PVA nanofibrous membranes via coaxial electrostatic spinning. The treatment using adenosine was based on our discovery that adenosine could promote the osteogenic ability of BMSCs by activating the STAT3 signaling pathway and exert a negative effect on the osteoclastogenesis of osteoclast precursors. The *in vivo* tests clearly demonstrate that PCL/PVA coaxial membrane is a promising system for the sustained-release of adenosine to restore large bone defects void of side effects, especially the undesirable hypotension and bradycardia, induced by systemic administration of adenosine.

Declaration of Competing Interest

The authors declare no competing financial interest.

Acknowledgements

This work was mainly supported by National Natural Science Foundation of China (51873157, 81771051 and 81800943), and partially supported by the Natural Science Foundation of Hubei Province of China (No.2018CFB497).

Appendix A. Supplementary data

Supplementary data to this article can be found online at https://doi.org/10.1016/j.jconrel.2019.12.048.

References

[1] V. Kumar, Adenosine as an endogenous immunoregulator in cancer pathogenesis: where to go? Purinerg. Signal 9 (2013) 145–165.
[2] M. Duarte-Araujo, C. Nascimento, M. Alexandrina Timoteo, T. Magalhaes-Cardoso, P. Correia-de-Sa, Dual effects of adenosine on acetylcholine release from myenteric motoneurons are mediated by junctional facilitatory a(2A) and extrajunctional inhibitory A(1) receptors, Brit. J. Pharmacol. 141 (2004) 925–934.
[3] P. Correia-de-Sa, S. Adaes, M.A. Timoteo, C. Vieira, T. Magalhaes-Cardoso, C. Nascimento, M. Duarte-Araujo, Fine-tuning modulation of myenteric motoneurons by endogenous adenosine: on the role of secreted adenosine deaminase, Auton. Neurosci. 126-127 (2006) 211–224.
[4] L.C. Strazzulla, B.N. Cronstein, Regulation of bone and cartilage by adenosine signaling, Purinerg. Signal 12 (2016) 583–593.
[5] T.V. Dunwiddie, Adenosine and suppression of seizures, Adv. Neurol. 79 (1999) 1001–1010.
[6] D. Boison, L. Scheurer, V. Zumsteg, T. Rulicke, P. Litynski, B. Fowler, S. Brandner, H. Mohler, Neonatal hepatic steatosis by disruption of the adenosine kinase gene, Proc. Natl. Acad. Sci. U. S. A. 99 (2002) 6985–6990.
[7] H. Takahama, T. Minamino, H. Asanuma, M. Fujita, T. Asai, M. Wakeno, H. Sasaki, H. Kikuchi, K. Hashimoto, N. Oku, M. Asakura, J. Kim, S. Takashima, K. Komamura, M. Sugimachi, N. Mochizuki, M. Kitakaze, Prolonged targeting of ischemic/reperfused myocardium by liposomal adenosine augments cardioprotection in rats, J. Am. Coll. Cardiol. 53 (2009) 709–717.
[8] G.G. Yegutkin, Nucleotide- and nucleoside-converting ectoenzymes: important modulators of purinergic signalling cascade, Biochim. Biophys. Acta 1783 (2008) 673–694.
[9] A.V. Sauer, M. Emanuela, H. Raisa Jofra, Z. Elena, C. Francesco, C. Miriam, G. Eyal, C.M. Roifman, M.C. Cervi, A. Alessandro, ADA-deficient SCID is associated with a specific microenvironment and bone phenotype characterized by RANKL/OPG imbalance and osteoblast insufficiency, Blood 114 (2009) 3216–3226.
[10] V.L. Kolachala, R. Bajaj, M. Chalasani, S.V. Sitaraman, Purinergic receptors in gastrointestinal inflammation, Am. J. Physiol. Gastrointest. Liver Physiol. 294 (2008) G401–G410.
[11] M. Zamani, M.P. Prabhakaran, S. Ramakrishna, Advances in drug delivery via electrospun and electrosprayed nanomaterials, Int. J. Nanomedicine 2013 (2013) 2997–3017.
[12] A. Saraf, L.S. Baggett, R.M. Raphael, F.K. Kasper, A.G. Mikos, Regulated non-viral gene delivery from coaxial electrospun fiber mesh scaffolds, J. Control. Release 143 (2010) 95–103.
[13] G. Cheng, C. Yin, H. Tu, S. Jiang, Q. Wang, X. Zhou, X. Xing, C. Xie, X. Shi, Y. Du, Controlled co-delivery of growth factors through layer-by-layer assembly of core-shell nanofibers for improving bone regeneration, ACS Nano 13 (2019) 6372–6382.
[14] J. Yoon, H.-S. Yang, B.-S. Lee, W.-R. Yu, Recent Progress in coaxial electrospinning: new parameters, various structures, and wide applications, Adv. Mater. 30 (2018) 1704765.
[15] L. Dan, J.T. Mccann, X. Younan, Use of electrospinning to directly fabricate hollow nanofibers with functionalized inner and outer surfaces, Small 1 (2010) 83–86.
[16] S. Torres-Giner, A. Martinez-Abad, J.V. Gimeno-Alcañiz, M.J. Ocio, J.M. Lagaron, Controlled delivery of gentamicin antibiotic from bioactive electrospun polylactide-based ultrathin fibers, Adv. Eng. Mater. 14 (2012) B112–B122.
[17] Y. Su, Q. Su, W. Liu, M. Lim, J.R. Venugopal, X. Mo, S. Ramakrishna, S.S. Al-Deyab, M. El-Newehy, Controlled release of bone morphogenetic protein 2 and dexamethasone loaded in core–shell PLLACL–collagen fibers for use in bone tissue engineering, Acta Biomater. 8 (2012) 763–771.
[18] Z. Zarekhalili, S.H. Bahrami, M. Ranjbar-Mohammadi, P.B. Milan, Fabrication and characterization of PVA/gum tragacanth/PCL hybrid nanofibrous scaffolds for skin substitutes, Int. J. Biol. Macromol. 94 (2017) 679–690.
[19] G. Cheng, J. Chen, Q. Wang, X. Yang, Y. Cheng, Z. Li, H. Tu, H. Deng, Z. Li, Promoting osteogenic differentiation in pre-osteoblasts and reducing tibial fracture healing time using functional nanofibers, Nano Res. 11 (2018) 3658–3677.
[20] Y. Zhang, M. Chang, F. Bao, M. Xing, E. Wang, Q. Xu, Z. Huan, F. Guo, J. Chang, Multifunctional Zn doped hollow mesoporous silica/polycaprolactone electrospun membranes with enhanced hair follicle regeneration and antibacterial activity for wound healing, Nanoscale 11 (2019) 6315–6333.
[21] X. Feng, J. Li, X. Zhang, T. Liu, J. Ding, X. Chen, Electrospun polymer micro/nanofibers as pharmaceutical repositories for healthcare, J. Control. Release 302 (2019) 19–41.
[22] S.M. Saeed, H. Mirzadeh, M. Zandi, J. Barzin, Designing and fabrication of curcumin loaded PCL/PVA multi-layer nanofibrous electrospun structures as active wound dressing, Prog. Biomater. 6 (2017) 39–48.
[23] M.F. Abazari, F. Soleimanifar, M. Nouri Aleagha, S. Torabinejad, N. Nasiri, G. Khamisipour, J. Amini Mahabadi, H. Mahboudi, S.E. Enderami, E. Saburi, J. Hashemi, M. Kehtari, PCL/PVA nanofibrous scaffold improve insulin-producing cells generation from human induced pluripotent stem cells, Gene 671 (2018) 50–57.
[24] T. Wu, G. Wang, X. Zhu, P. Liu, Z. Xian, H. Zhang, Y. Zhang, H. Zhao, Growth and in situ transformation of TiO2 and HTiOF3 crystals on chitosan-polyvinyl alcohol copolymer substrates under vapor phase hydrothermal conditions, Nano Res. 9 (2016) 745–754.
[25] B. Gu, F. Papadimitrakopoulos, D.J. Burgess, PLGA microsphere/PVA hydrogel coatings suppress the foreign body reaction for 6 months, J. Control. Release 289 (2018) 35–43.
[26] B.B. Fredholm, I.J. AP, K.A. Jacobson, J. Linden, C.E. Muller, International Union of Basic and Clinical Pharmacology. LXXXI. Nomenclature and classification of adenosine receptors—an update, Pharmacol. Rev. 63 (2011) 1–34.
[27] E.S.L. Chan, B.N. Cronstein, Methotrexate—how does it really work? Nat. Rev. Rheumatol. 6 (2010) 175–178.
[28] A. Mediero, M. Perez-Aso, T. Wilder, B.N. Cronstein, Brief report: methotrexate prevents Wear particle-induced inflammatory osteolysis in mice via activation of adenosine a 2A receptor: MTX prevents inflammatory osteolysis via a 2A receptor, Arthritis Rheumatol. 67 (2015) 849–855.
[29] T.L. Aghaloo, T. Chaichanasakul, O. Bezouglaia, B. Kang, R. Franco, S.M. Dry, E. Atti, S. Tetradis, Osteogenic potential of mandibular vs. long-bone marrow stromal cells, J. Dent. Res. 89 (2010) 1293–1298.
[30] X. Cheng, Q.L. Wan, Z.B. Li, AG490 suppresses interleukin-34-mediated osteoclastogenesis in mice bone marrow macrophages, Cell Biol. Int. 41 (2017) 659–668.
[31] G. Cheng, Y. Du, X. Ma, J. Li, Y. Cheng, Y. Cao, Z. Wang, X. Shi, H. Deng, Z. Li, Incorporating platelet-rich plasma into coaxial electrospun nanofibers for bone tissue engineering, Int. J. Pharm. 547 (2018) 656–666.
[32] H. Kang, Y.R.V. Shih, M. Nakasaki, H. Kabra, S. Varghese, Small molecule–driven direct conversion of human pluripotent stem cells into functional osteoblasts, Sci. Adv. 2 (2016) (e1600691-e1600691).
[33] S.M. Holland, F.R. Deleo, H.Z. Elloumi, A.P. Hsu, U. Gulbu, B. Nina, A.F. Freeman, D. Andrew, D. Joie, M.L. Turner, STAT3 mutations in the hyper-IgE syndrome, N. Engl. J. Med. 357 (2007) 1608–1619.
[34] J.E. Darnell, STATs and gene regulation, Science 277 (1997) 1630–1635.
[35] X. Yu, Z. Li, Q. Wan, X. Cheng, J. Zhang, J.L. Pathak, Z. Li, Inhibition of JAK2/STAT3 signaling suppresses bone marrow stromal cells proliferation and osteogenic differentiation, and impairs bone defect healing, Biol. Chem. 399 (2018) 1313–1323.
[36] M. Katebi, M. Soleimani, B.N. Cronstein, Adenosine A2A receptors play an active role in mouse bone marrow-derived mesenchymal stem cell development, J. Leukoc. Biol. 85 (2009) 438–444.
[37] B. Gharibi, A.A. Abraham, J. Ham, B.A. Evans, Adenosine receptor subtype expression and activation influence the differentiation of mesenchymal stem cells to osteoblasts and adipocytes, J. Bone Miner. Res. 26 (2011) 2112–2124.
[38] S.H. Carroll, N.A. Wigner, N. Kulkarni, H. Johnston-Cox, L.C. Gerstenfeld, K. Ravid, A2B adenosine receptor promotes mesenchymal stem cell differentiation to osteoblasts and bone formation in vivo, J. Biol. Chem. 287 (2012) 15718–15727.
[39] A. Cappariello, A. Maurizi, V. Veeriah, A. Teti, Reprint of: the great beauty of the osteoclast ☆ ☆☆, Arch. Biochem. Biophys. 561 (2014) 13–21.
[40] E.M. Pritchard, C. Szybala, D. Boison, D.L. Kaplan, Silk fibroin encapsulated powder reservoirs for sustained release of adenosine, J. Control. Release 144 (2010) 159–167.
[41] S. Suzuki, T.-A. Asoh, A. Kikuchi, Design of core-shell gel beads for time-programmed protein release, J. Biomed. Mater. Res. A 101A (2013) 1345–1352.
[42] W. Chun-Yang, L. Jun-Jian, F. Cun-Yi, M. Xiu-Mei, R. Hong-Jiang, L. Feng-Feng, The effect of aligned core-shell nanofibres delivering NGF on the promotion of sciatic nerve regeneration, J. Biomater. Sci-Polym. E. 23 (2012) 167–184.
[43] J. Lu, W. Zhuang, L. Li, B. Zhang, L. Yang, D. Liu, H. Yu, R. Luo, Y. Wang, Micelle-embedded layer-by-layer coating with catechol and phenylboronic acid for tunable drug loading, sustained release, mild tissue response, and selective cell fate for re-

endothelialization, ACS Appl. Mater. Interfaces 11 (2019) 10337–10350.
[44] D. Wei, R. Qiao, J. Dao, J. Su, C. Jiang, X. Wang, M. Gao, J. Zhong, Soybean lecithin-mediated nanoporous PLGA microspheres with highly entrapped and controlled released BMP-2 as a stem cell platform, Small 14 (2018) e1800063.
[45] Y.F. Tan, L.L. Lisa, X.G. Minru, V. Subbu, Controlled-release nanotherapeutics: state of translation, J. Control. Release 284 (2018) 39–48.
[46] R.M. Salasznyk, W.A. Williams, A. Boskey, A. Batorsky, G.E. Plopper, Adhesion to vitronectin and collagen I promotes osteogenic differentiation of human mesenchymal stem cells, J. Biomed. Biotechnol. 2004 (2004) 24–34.
[47] M. Mizuno, Y. Kuboki, Osteoblast-related gene expression of bone marrow cells during the osteoblastic differentiation induced by type I collagen, J. Biochem. 129 (2001) 133–138.
[48] M. Mahaffey, Adenosine as an adjunct to thrombolytic therapy for acute myocardial infarction: results of a multicenter, randomized, placebo-controlled trial : the Acute Myocardial Infarction STudy of ADenosine (AMISTAD) trial, J. Am. Coll. Cardiol. 34 (1999) 1711–1720.
[49] A.M. Ross, R.J. Gibbons, G.W. Stone, R.A. Kloner, R.W. Alexander, A randomized, double-blinded, placebo-controlled multicenter trial of adenosine as an adjunct to reperfusion in the treatment of acute myocardial infarction (AMISTAD-II), J. Am. Coll. Cardiol. 45 (2005) 1775–1780.
[50] M.B. Forman, G.W. Stone, E.K. Jackson, Role of adenosine as adjunctive therapy in acute myocardial infarction, Cardiovasc. Drug Rev. 24 (2006) 116–147.
[51] I.I. Mathews, M.D. Erion, S.E. Ealick, Structure of human adenosine kinase at 1.5 A resolution, Biochemistry 37 (1998) 15607–15620.